Simulation of Wave-Plus-Current Scour beneath Submarine Pipelines

Bjarke Eltard Larsen[1]; David R. Fuhrman[2]; and B. Mutlu Sumer[3]

Abstract: A fully coupled hydrodynamic and morphologic numerical model was utilized for the simulation of wave-plus-current scour beneath submarine pipelines. The model was based on incompressible Reynolds-averaged Navier–Stokes equations, coupled with k-ω turbulence closure, with additional bed and suspended load descriptions forming the basis for seabed morphology. The model was successfully validated against experimental measurements involving scour development and eventual equilibrium in pure-current flows over a range of Shields parameters characteristic of both clear-water and live-bed regimes. This validation complements previously demonstrated accuracy for the same model in simulating pipeline scour processes in pure-wave environments. The model was subsequently utilized to simulate combined wave-plus-current scour over a wide range of combined Keulegan–Carpenter numbers and relative current strengths. The resulting equilibrium scour depths and trends were shown to be in accordance with existing experimentally based expressions from the literature. The variety of scour profile types emerging under various flow conditions is detailed and reconciled with experimental observations. The resulting matrix of scour depth time series was systematically analyzed, resulting in a new generalized expression for the scour time scale in combined wave-plus-current flow environments. This expression is fully consistent with existing experimentally based relations at both pure-current and pure-wave limits and is appropriate for engineering use. **DOI: 10.1061/(ASCE)WW.1943-5460.0000338.**

Author keywords: Scour; Pipelines; Sediment transport; Morphology; Combined waves and current; Timescale; Turbulence modeling; k-ω model.

Introduction

Scour beneath submarine pipelines has been the subject of much research (see Hoffmans and Verheij 1997; Whitehouse 1998; Sumer and Fredsøe 2002 for a general introduction). Most research has been in the form of laboratory experiments, although in more recent years, a large number of numerical investigations have emerged as computational power has increased. The earliest attempts to model scour beneath pipelines were made using potential flow models, whereas more recent attempts were carried out by solving the complete Navier–Stokes equations, either in the form of the Reynolds-averaged Navier–Stokes equations (RANS) or using large-eddy simulation (LES). Brørs (1999), Liang and Cheng (2005b), Liang et al. (2005), Zhao and Fernando (2007), and Zanganeh et al. (2012) succeeded in modeling the scour evolution beneath pipelines in steady currents, and Liang and Cheng (2005a), Kazeminezhad et al. (2012), and Fuhrman et al. (2014) modeled the scour beneath a pipeline as a result of waves. Fuhrman et al. (2014) demonstrated accurate scour time scales while also managing to simulate the backfilling process caused by a change to milder wave conditions.

To date, most research (both numerical and experimental) has focused on scour induced by either pure waves or currents, whereas comparatively few studies have involved combined wave-plus-current environments. Of these, Lucassen (1984) carried out a series of experiments for a rather limited set of waves and currents, whereas Sumer and Fredsøe (1996) carried out scour depth investigations for a comprehensive range of combined waves and currents. The experimental studies focused primarily on the equilibrium scour depth, thus little is known regarding the timescale of scour in generalized wave-plus-current cases. More recently, Myrhaug et al. (2009) focused on scour depth below pipelines resulting from second-order random waves plus currents, and Cheng et al. (2014) investigated the scour propagation speed along the length of the pipeline. Numerically, wave-plus-current scour beneath pipelines has only been investigated using potential flow models (e.g., Bernetti et al. 1990; Hansen 1992).

The present study focused on the numerical simulation of wave-plus-current–induced scour beneath submarine pipelines, based on a model solving RANS equations, fully coupled with turbulence closure, bed and suspended load sediment transport descriptions, and a seabed morphological model. The motivation is threefold. Because wave-plus-current scour has yet to be simulated in a fully coupled numerical model, the first goal was to establish detailed model accuracy in accordance with the steady-flow experiments of Mao (1986), as well as for equilibrium scour depths in accordance with the wave-plus-current experiments of Sumer and Fredsøe (1996). The second goal was to investigate the scour process in detail, shedding light on the variety of equilibrium scour profiles that may emerge under various flow conditions. Third, the authors wished to quantify the pipeline scour timescale for generalized

[1]Ph.D. Student, Technical Univ. of Denmark, Dept. of Mechanical Engineering, Section of Fluid Mechanics, Coastal and Maritime Engineering, DK-2800 Kongens, Lyngby, Denmark (corresponding author). E-mail: bjelt@mek.dtu.dk

[2]Associate Professor, Technical Univ. of Denmark, Dept. of Mechanical Engineering, Section of Fluid Mechanics, Coastal and Maritime Engineering, DK-2800 Kongens, Lyngby, Denmark.

[3]Professor Emeritus, Technical Univ. of Denmark, Dept. of Mechanical Engineering, Section of Fluid Mechanics, Coastal and Maritime Engineering, DK-2800 Kongens, Lyngby, Denmark.

Note. This manuscript was submitted on May 26, 2015; approved on January 28, 2016; published online on March 15, 2016. Discussion period open until August 15, 2016; separate discussions must be submitted for individual papers. This paper is part of the ***Journal of Waterway, Port, Coastal, and Ocean Engineering***, © ASCE, ISSN 0733-950X.

wave-plus-current environments. The goal was to formulate an analytical physically based expression for this quantity that is fully consistent with existing expressions at both pure-wave and pure-current limits.

Model Description

In this section the utilized model is briefly described. As the model has already been described in detail by Fuhrman et al. (2014) the reader is referred to this work for further details. The flow is simulated by solving the incompressible Reynolds-averaged Navier-Stokes equations (RANS) and the continuity equation, coupled with the two-equation k-ω turbulence model by Wilcox (2006, 2008) for closure.

Model boundary conditions are as follows. Friction wall boundaries (i.e., the pipeline and the seabed) utilize a no-slip condition such that velocities are zero. The top boundary is modeled as a frictionless lid, meaning that vertical velocities are set to zero, and horizontal velocities and scalar hydrodynamic quantities have zero gradient. This means that the top boundary does not represent the free surface of real waves. At the bottom boundary, a hydraulically rough wall is assumed, with the friction velocity (U_f) determined from the tangential velocity at the nearest cell center based on an assumed logarithmic velocity distribution. The friction velocity is then used to calculate k and ω in the cell nearest to the wall with standard wall functions as described by Fuhrman et al. (2014). The pipeline surface is modeled as a hydraulically smooth wall, utilizing a generalized wall function approach based on the profile of Cebeci and Chang (1978) as also detailed by Fuhrman et al. (2014).

The flow is driven by a Dirichlet condition, i.e., a specified velocity at the left-hand inlet boundary, which comes from a separate one-dimensional vertical (1DV) pure boundary layer simulation, made utilizing the same model as described earlier. In this boundary layer simulation, the flow is driven by a body force given by

$$F = U_m \frac{2\pi}{T_w} \cos\left(\frac{2\pi}{T_w} t\right) + \frac{U_{fc}^2}{h} \tag{1}$$

where U_m = maximum free stream velocity of the oscillating flow; T_w = wave period; U_{fc} = desired friction velocity of the current alone; t = time; and h = domain height. The simulation is continued until a periodic repetitive state is reached. From here, the velocity profile as well as the profiles for k and ω are sampled over a single period, and are then repeated periodically as inlet boundary conditions within the scour simulations. Through this approach, the special characteristics of the combined wave–current boundary layer are incorporated directly within the driving inlet flow (e.g., the well-known apparent roughness effect of a turbulent wave boundary layer on the current; see e.g., Fredsøe et al. 1999). At the same time, the computational time required is kept low, because the long time required (hundreds to thousands of periods) to achieve a fully developed wave-plus-current flow is simulated entirely within the 1DV framework.

The model for the bed-load transport corresponds to that of Roulund et al. (2005), who extended the model of Engelund and Fredsøe (1976) to also include three-dimensional effects as well as bed slope modifications to the Shields parameter. The suspended load is calculated by solving the advection-diffusion equation for the concentration (see Fredsøe and Deigaard 1992, p. 238). The equation for the suspended sediment is solved on a subset of the main computational mesh, where the near-bed cells below a given reference level (b) are removed. At this reference level, a reference concentration (c_b,) boundary condition is imposed. There are several formulations of c_b, but the one by Engelund and Fredsøe (1976) is utilized here.

The morphological updating routine is based on the sediment continuity (Exner) equation as described by Jacobsen et al. (2014). The Exner equation is based on instantaneous sediment transport fields, and therefore, the morphological and hydrodynamic times are equivalent. To ensure that the bed slopes do not exceed the angle of repose, the sand-slide model described in detail by Roulund et al. (2005) is implemented. In the present work, this model was activated at positions where the local bed angle exceeds the angle of repose ($\phi_s = 32°$), and was deactivated once the local bed angle was reduced to 31.9°.

The equations comprising the fully coupled model outlined earlier are solved numerically using the open-source computational fluid dynamics (CFD) toolbox *OpenFOAM*, version 1.6-ext, making use of a finite-volume spatial discretization with a collocated variable arrangement, in conjunction with a standard pressure implicit with splitting of operators (PISO) algorithm. For further details, see Jacobsen et al. (2014). As noted previously, the fully coupled model presented earlier has also been utilized recently by Fuhrman et al. (2014) in the simulation of wave-induced scour beneath submarine pipelines, as well as by Baykal et al. (2015), who simulated the current-induced scour process around a vertical monopile cylinder. The hydrodynamic model can likewise be considered a single-phase variant of the two-phase (air–water) model presented in Jacobsen et al. (2012).

Model Setup

For all forthcoming simulations, the height of the domain has been set to $h = 10D$, where D is the pipeline diameter. The horizontal span has, in most cases, been set to $-20D \leq x \leq 20D$, but has gradually been changed to $-15D \leq x \leq 40D$ for cases involving strong mean currents, as this promotes more asymmetric scour profiles. The pipeline is placed on the bed with its bottom at the origin $(x,y) = (0,0)$. For numerical reasons, an initial scour hole is needed to provide space for computational cells beneath the pipeline. The initial hole is sinusoidal with a depth of $S_0/D = 0.15$. The computational mesh is graded, such that near the pipeline, the smallest cells have height equal to $0.003D$, whereas at the seabed cells are set to have a height $0.5d$, d being the grain-size diameter. Between the pipeline and the bed, different mesh gradings were used. Experience has shown that rapidly deepening scour holes can distort the mesh, and to combat this, it has been necessary to increase the mesh resolution in certain cases where this proved problematic. This has resulted in computational domains having a cell count between 8,732 and 18,134. In Fig. 1, typical mesh in the near vicinity of the pipeline is shown as an example.

Validation

In this section, the numerical model described earlier is validated for scour depth and profile development beneath pipelines subject to steady current flow. For further validation of the present model, see the recent work of Fuhrman et al. (2014), who accurately simulated pure wave-induced scour and backfilling processes utilizing the same model. Here, the model results are compared with those presented by Mao (1986). Mao (1986) tested current-induced scour development in both clear-water and live-bed regimes. These experiments provide an excellent benchmark, as scour profiles are available throughout the development, enabling

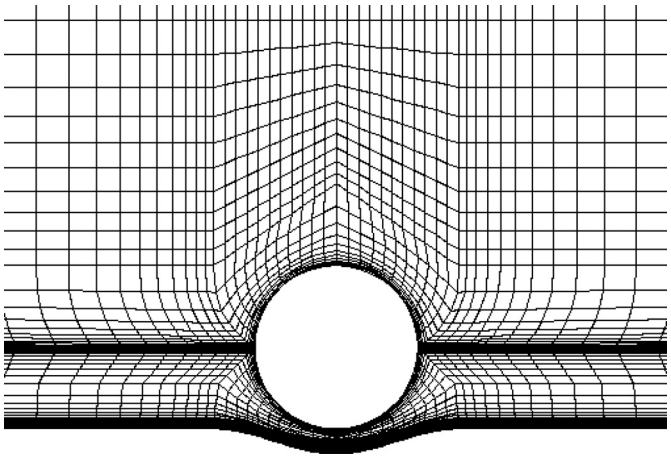

Fig. 1. Example of the computational mesh used for the scour cases

detailed comparison of the simulated and experimental scour processes and development.

Mao (1986) presents results for current-induced scour with a pipeline diameter (D) of 0.1 m and a sediment grain size (d) of 0.36 mm, for cases yielding far-field Shields parameter

$$\theta = \frac{\tau_b}{\rho g(s-1)d} = \frac{U_f^2}{(s-1)gd} = 0.048 \tag{2}$$

for the clear-water case, and $\theta = 0.098$ for the live-bed case. Here, τ_b is the bed-shear stress, g is the gravitational acceleration, and $s = 2.65$ is the relative sediment density. For the purposes of the present validation, the authors aim to effectively maintain Shields parameter similarity with the cases of Mao (1986), while utilizing (hence directly validating) the same computational mesh as in the forthcoming wave-plus-current scour simulations (i.e., with $D = 0.03$ m and $d = 0.19$ mm). Thus, the experimental results from Mao (1986) are compared in terms of length scales (hence scour depth) normalized by the pipeline diameter, and in terms of dimensionless morphological time defined by

$$t^* = \frac{\sqrt{g(s-1)d^3}}{D^2} t \tag{3}$$

which accounts for the cross-sectional area of the scour hole scaling as D^2. Here, t is the physical time. Such comparison is justified in a nondimensional sense, because the expected equilibrium scour depth-to-pipeline diameter ratio is well known to be approximately constant (Sumer and Fredsøe 1990)

$$\frac{S_e}{D} = 0.6 \pm 0.2 \tag{4}$$

whereas the dimensionless timescale of the scour development depends only on θ (Fredsøe et al. 1992). For physical consistency, in the simulation of the clear-water case, the Shields parameter was slightly reduced to $\theta = 0.044$ to ensure that the far-field Shields parameter is indeed below the critical value ($\theta_c = 0.045$) assumed in the model formulation.

The steady current flows are driven from the inlet as described previously, based on results from a prior 1DV simulation driven by the body force [Eq. (1)] with $U_m = 0$ (i.e., no waves) and with friction velocity (U_{fc}) chosen to yield the desired θ according to Eq. (2). Because an initial scour hole is specified in the model,

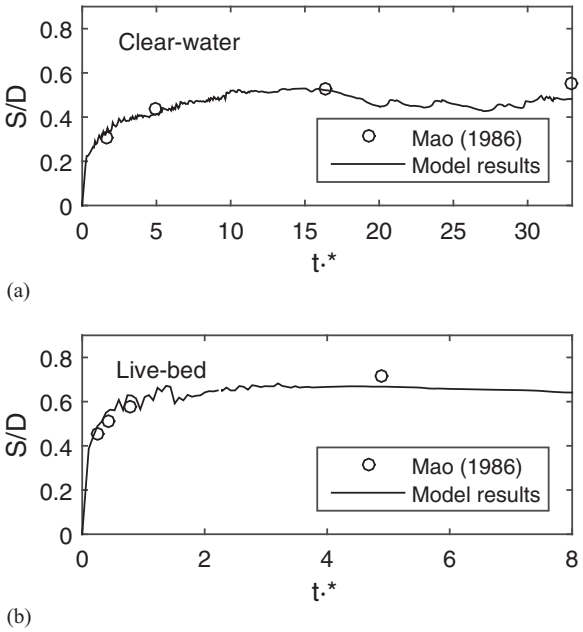

Fig. 2. Comparison of modeled and experimental nondimensional scour depth; experimental data taken from Mao (1986): (a) clear water, with $\theta = 0.048$ and $D = 0.1$ m in the experiments and $\theta = 0.044$ and $D = 0.03$ m in the model results; (b) live bed, with $\theta = 0.098$ and $D = 0.1$ m in the experiments and $\theta = 0.098$ and $D = 0.03$ m in the model results

whereas the experiments by Mao (1986) started from a plane bed, it is necessary to compensate for the approximate time required to achieve the initial scour depth. This was achieved by evaluating the initial simulated rate of scour (dS/dt) and extrapolating back in time to $S = 0$, leading to a shifted time given by $t'^* = t^* + t^*_{\text{shift}}$. For the validation cases, a warm-up period of $t = 30$ s is utilized, during which the morphology is switched off, and the hydrodynamic and sediment transport fields are allowed to become fully developed. At the end of this warm-up period the morphology is switched on, with this time denoted as $t = 0$.

In Fig. 2, the time series of the nondimensional scour depth, taken as the vertical clearance beneath the center of the pipeline, is shown as a function of nondimensional time for both the clear-water [Fig. 2(a)] and the live-bed [Fig. 2(b)] regimes. Also included in the figure are the temporal scour depth measurements from the experiments of Mao (1986). In both cases, most of the scour occurs relatively quickly, followed by a slow increase in the scour depth until equilibrium is reached. This figure shows that the model predicts similar scour evolution, as well as equilibrium scour depths, as in the experiments. In both clear-water and live-bed regimes, the predicted equilibrium scour is slightly below that observed experimentally.

As further validation, the computed and measured (Mao 1986) scour profiles at various nondimensional times are compared in Fig. 3, for both the clear-water [(a), (c), and (e)] and live-bed [(b), (d), and (f)] cases. Again, in both cases, it can be seen that most of the scour occurs rapidly, as the scour is already appreciable in the earliest snapshots. Alternatively, the increase in scour width and the migration of the downstream shoulder require a substantially longer time. The first phase of the observed scour corresponds to tunnel erosion, where a large amount of water is forced through the small gap between the pipeline and the bed, resulting in large amplification of the bed shear stress and thus a rapid increase in the scour

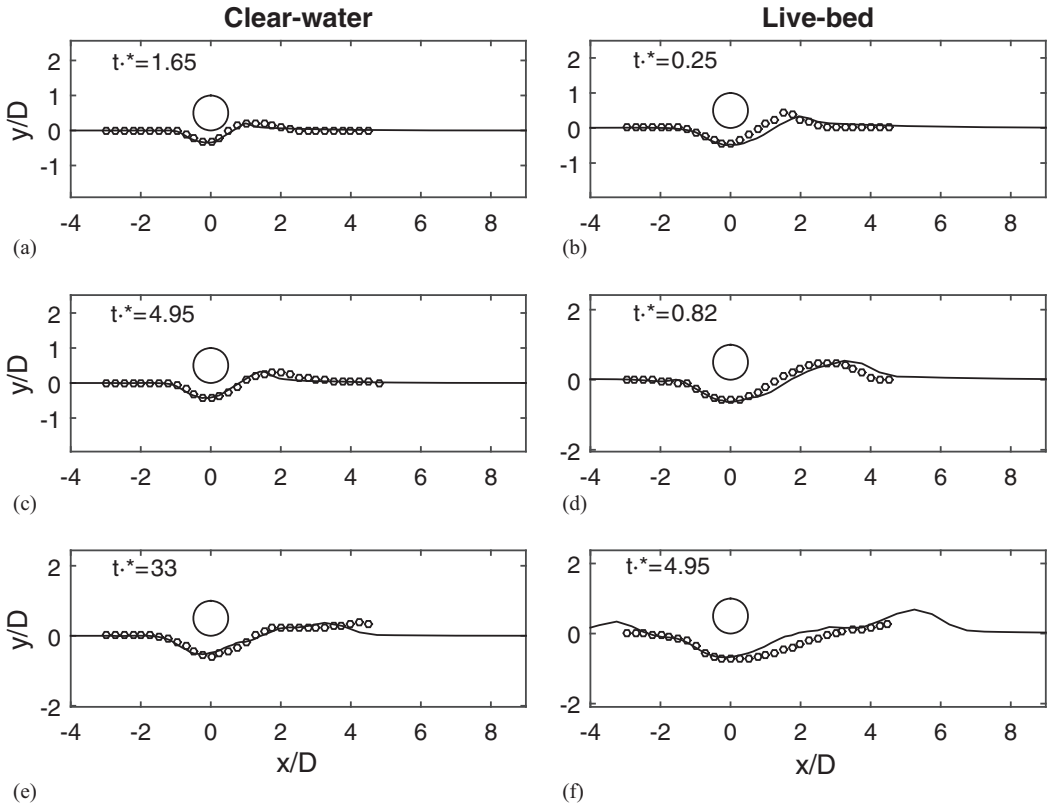

Fig. 3. Comparison of modeled (circles) and experimental (lines) scour profiles at different times; experimental data taken from Mao (1986): (a, c, and e) clear water, with $\theta = 0.048$ and $D = 0.1$ m in the experiments and $\theta = 0.044$ and $D = 0.03$ m in the model results; (b, d, and f) live bed, with $\theta = 0.098$ and $D = 0.1$ m in the experiments and $\theta = 0.098$ and $D = 0.03$ m in the model results

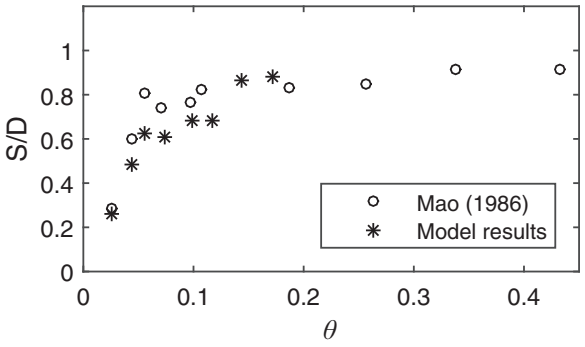

Fig. 4. Equilibrium scour depth versus Shields parameter for both experimental [data taken from Mao (1986), with $\theta \approx 0.03 - 0.43$ and $D = 0.05 - 0.1$ m] and modeled (with $\theta = 0.026$–0.172 and $D = 0.03$ m)

depth. The second corresponds to the lee-wake erosion phase, where vortices convect sediment downstream. The model results compare quite well with the experimental results from Mao (1986) throughout both phases, as seen by the consistently good profile match in Fig. 3. Hence, this comparison demonstrates the ability of the model to capture not only the scour depth evolution, but also the bed profile morphology in both the clear-water and live-bed cases. Note that in the live-bed case, a small difference can, however, be seen at $t'^* = 4.95$ [Fig. 3(f)]. This can be attributed to the formation of bedforms developing upstream of the pipeline, which shield the flow. Although deviating slightly from the observed profile in this detail, it is emphasized that the development of such bedforms is, in fact, an expected physical phenomenon in the live-bed regime. The authors regard the resemblance in the computed results and the experiments by Mao (1986) as still acceptable, even at this later stage in the profile development.

As a final test of the model accuracy, a number of additional steady-current scour cases were simulated to systematically check the Shields parameter dependence on the equilibrium scour depth with that evident from the experiments of Mao (1986). For this purpose, six additional values ($\theta = 0.026$, 0.055, 0.073, 0.117, 0.143, and 0.172) were selected and simulated until equilibrium scour was reached, as before. The resulting equilibrium scour depths for all (eight) cases considered were then plotted as a function of θ in Fig. 4, as were the experimental results reported by Mao (1986). This figure shows that the computed equilibrium scour depth dependence resembles that of Mao (1986) over the full range of θ considered, starting within the clear-water regime and extending well into the live-bed regime. The scour depth in the experiments reaches an equilibrium value of $S/D \approx 0.8$–0.9 at slightly lower θ than predicted by the model. For low values of θ, the equilibrium scour depths match the experimentally based empirical expression [Eq. (4)] quite well, whereas for $\theta > 0.15$, the scour depths are slightly larger, around $S/D \approx 0.9$. This is generally consistent with the results from Mao (1986). As seen, all of the computed and experimental results for the live-bed equilibrium scour are within 1–1.5 standard deviations of the mean predicted by Eq. (4).

Based on the previously presented results, the model has demonstrated the ability to reliably predict current-induced scour processes beneath a submarine pipeline, both in terms of the equilibrium scour depths as well as the resulting morphological development of the surrounding bed profile. These results are complemented by those presented previously by Fuhrman et al. (2014).

Table 1. Summary of Cases Considered for Wave-Plus-Current–Induced Scour beneath Submerged Pipelines

KC	T_w (s)	U_m (m/s)	U_c (m/s)	m	θ_{cw}
5.6	1.10	0.153	0–0.357	0–0.7	0.119–0.327
11	1.22	0.240	0–0.360	0–0.6	0.177–0.432
15	2.50	0.177	0–0.413	0–0.7	0.088–0.386
19.6	3.00	0.196	0–0.457	0–0.7	0.092–0.464
21.1	2.64	0.239	0–0.558	0–0.7	0.120–0.681
25.3	3.51	0.216	0–0.504	0–0.7	0.110–0.550
30	3.50	0.257	0–0.600	0–0.7	0.120–0.768
35	2.70	0.388	0–0.388	0–0.5	0.260–0.431
48	6.00	0.240	0–0.560	0–0.7	0.089–0.649
51	4.50	0.340	0–0.793	0–0.7	0.176–1.290

Note: All cases use pipeline diameter $D = 0.03$ m and grain diameter $d = 0.19$ mm.

Simulation of Wave-Plus-Current Scour

After collectively validating the model for both current-induced scour (aforementioned) as well as wave-induced scour (Fuhrman et al. 2014), it was then utilized for the numerical study of combined wave-plus-current scour processes beneath pipelines. In the following, the results of 77 new wave-plus-current scour cases are presented and analyzed. The cases considered consist of waves characterized by 10 different Keulegan–Carpenter numbers (KC)

$$KC = \frac{U_m T_w}{D} \tag{5}$$

and up to eight different values of the parameter m

$$m = \frac{U_c}{U_c + U_m} \tag{6}$$

which defines the relative strength of the current, i.e., $m = 0$ corresponds to pure-wave conditions, with $m = 1$ corresponding to pure-current conditions, where U_c is the current velocity at the center of the pipeline. The discrete values of the current are selected such that $m = 0, 0.1, 0.2, \ldots, 0.7$. The previously considered eight pure-current results will likewise be utilized to characterize $m = 1$. Table 1 shows a summary of the new cases, organized by their respective KC values. The table also provides the range of the far-field Shields parameter (θ_{cw}), which can be interpreted as the maximum Shields parameter of the combined wave–current flow, calculated by utilizing an equivalent to the formula given by Soulsby (1995)

$$\theta_{cw} = \theta_m + \theta_w \tag{7}$$

where

$$\theta_m = \theta_{\text{cur}}\left(1 + 1.2\left(\frac{\theta_w}{\theta_{\text{cur}} + \theta_w}\right)^{3.2}\right) \tag{8}$$

is the mean Shields parameter. Here, θ_{cur} is the Shields parameter coming from the current alone calculated from friction velocity U_{fc} [taken directly from the input of the boundary layer simulations, Eq. (1)] and θ_w is the maximum Shields parameter of the oscillating flow, calculated from the maximum friction velocity of the oscillating flow, taken as

$$U_{fw} = \sqrt{0.5 f_w} U_m \tag{9}$$

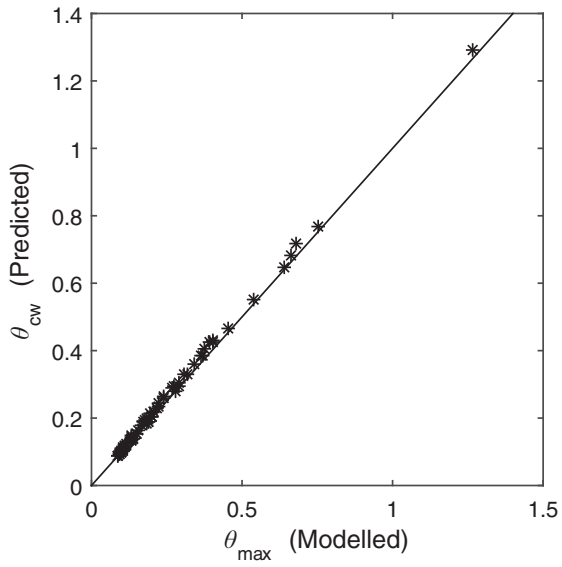

Fig. 5. Fit between maximum computed Shields parameters from the model and the predicted Shields parameters from Eq. (7) as proposed by Soulsby (1995)

For convenience, f_w is taken as the maximum of the laminar, smooth-turbulent, and rough-turbulent wave friction factors (i.e., $f_w = \max[f_w^{\text{lam}}, f_w^{\text{smooth}}, f_w^{\text{rough}}]$). For this purpose, f_w^{lam} is calculated theoretically as

$$f_w^{\text{lam}} = \frac{2}{\sqrt{\text{R}}} \tag{10}$$

f_w^{smooth} is calculated from the expression of Fredsøe and Deigaard (1992)

$$f_w^{\text{smooth}} = 0.035\text{R}^{-0.16} \tag{11}$$

where $\text{R} = U_m a/\nu$ is the Reynolds number, and the empirical expression from Fuhrman et al. (2013)

$$f_w^{\text{rough}} = \exp\left(5.5\left(\frac{a}{k_s}\right)^{-0.16} - 6.7\right) \tag{12}$$

is utilized for the rough-wall regime. To check that Eq. (7) is representative of the maximum computed Shields parameter, it is plotted as a function of the maximum far-field Shields parameters taken directly from the model in Fig. 5. This figure confirms that Eq. (7) is an excellent representation of the maximum far-field Shields parameter because a nearly perfect match is achieved.

Following the methodology of Fuhrman et al. (2014), for all cases considered, a warm-up period of $10T_w$ is used, during which time the morphology is switched off. This is again done to allow both the hydrodynamic and sediment transport fields to fully develop. At the end of the warm-up period, the morphology is switched on, this time denoted as $t = 0$.

Scour Time Series

For all cases, the scour depth (S), again taken directly beneath the pipeline center, was monitored. The simulations proceeded until an apparent equilibrium was reached (i.e., when the scour curve flattened and maintained a fairly constant value over a significant

duration). As examples, Figs. 6 and 7 show the computed nondimensional scour depth (S/D) as a function of nondimensional time (t^*) for cases with fixed $KC = 19.6$ and $KC = 30$ for each of the eight m values considered. It can be seen that the scour process begins immediately after the morphology is switched on, with the scour depth increasing until equilibrium is reached, similar to before. The computed equilibria are dynamic, rather than static, as the scour depth is seen to fluctuate slightly even after long-term trends have vanished.

The other KC numbers investigated demonstrate temporal scour developments quite similar to those shown in Figs. 6 and 7. The lone exceptions are cases with $KC = 11$ in combination with low values of m (i.e., weak currents), in which the temporal scour process typically follows two separate phases. The first resembles the usual evolution as in Figs. 6 and 7, which is then followed by a second phase of excessive scour. This behavior is consistent with that observed and detailed in the previous pure-wave simulations of Fuhrman et al. (2014) for $KC = 11$. They explained the second phase as part of a resonance phenomenon excited within the model, wherein profile wavelengths developing beneath the pipeline closely match those expected for vortex ripples in this KC range. As this phenomenon has already been explained and illustrated in detail by Fuhrman et al. (2014), for brevity, further details are not presented here. Following Fuhrman et al. (2014), however, for the four cases of $KC = 11$ with $m \le 0.3$ in which this behavior is evident, only the first simulated scour phase is considered in what follows, as this is seemingly consistent with what has been observed experimentally.

Equilibrium Scour Depth

Here, the computed equilibrium scour depths are compared with existing experimentally based empirical expressions from the literature. The equilibrium scour depths from all of the wave-plus-current model simulations, here taken as the average scour depth over several periods after the equilibrium scour depth has been reached, are summarized in Fig. 8 for the 10 different KC numbers combined with up to eight different values of m. Included as the full line in each subplot is the empirical relation given by Sumer and Fredsøe (1996)

$$S_e = S_c F \tag{13}$$

where S_c = equilibrium scour depth from the current alone [Eq. (4)]; and F is given by

$$F = \begin{cases} \frac{5}{3}(KC)^{a_m}\exp(2.3b_m), & 0 \le m \le 0.7 \\ 1, & m > 0.7 \end{cases} \tag{14}$$

where a_m and b_m depend on m according to

$$a_m = \begin{cases} 0.557 - 0.912(m - 0.25)^2, & 0 \le m \le 0.4, \\ -2.14m + 1.46, & 0.4 < m \le 0.7, \end{cases} \tag{15}$$

$$b_m = \begin{cases} -1.14 + 2.24(m - 0.25)^2, & 0 \le m \le 0.4, \\ 3.3m - 2.5, & 0.4 < m \le 0.7 \end{cases} \tag{16}$$

The additional dashed lines in Fig. 8 denote plus or minus the standard deviation (i.e., $\pm 0.2\ S_e/D$) about the mean equilibrium scour from Eq. (13), as implied by Eq. (4).

Generally, it can be seen that the modeled equilibrium scour depths for combined wave-plus-current flow compare reasonably with the experimentally based prediction [Eq. (13)] for all of the cases considered. This further validates the model for simulated wave-plus-current scour conditions. The general trend of the scour depth in relation to m is as follows. For low values of m, the scour

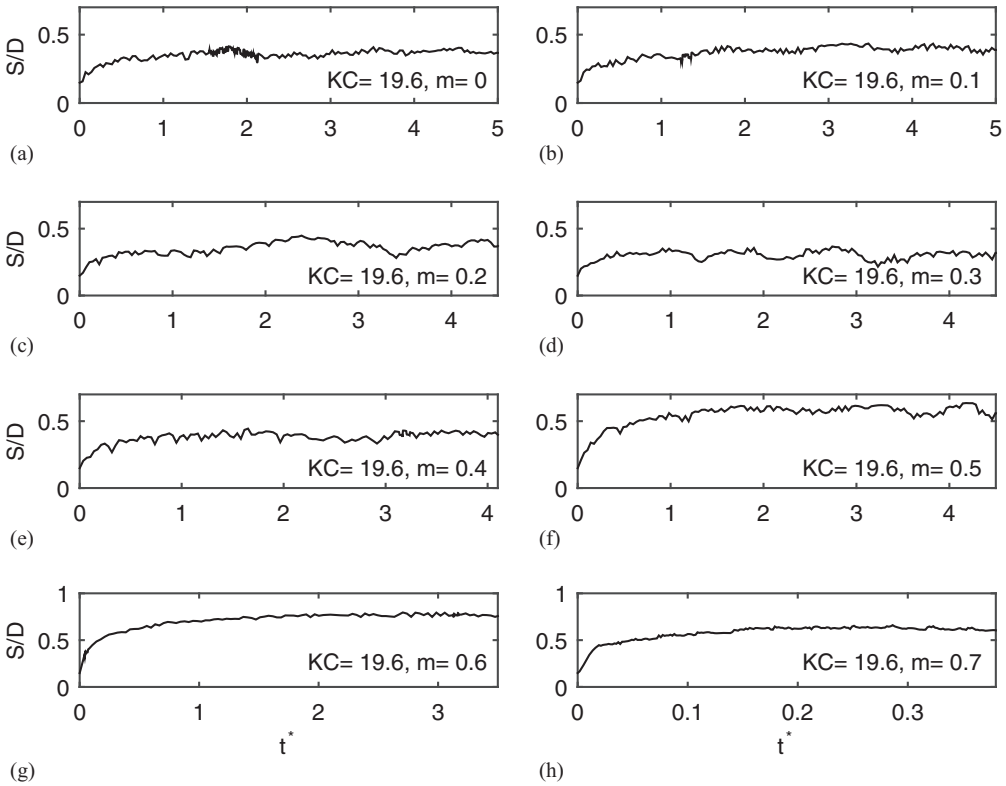

Fig. 6. Simulated scour development for combined wave-plus-current cases with fixed $KC = 19.6$ and different values of m

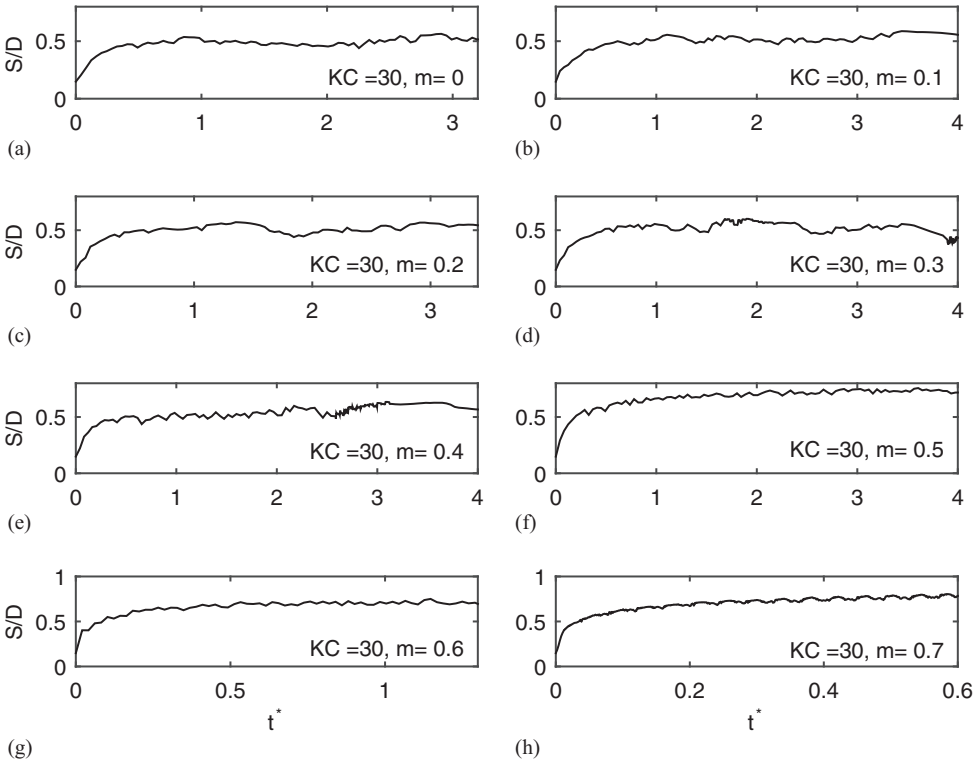

Fig. 7. Simulated scour development for combined wave-plus-current cases with fixed $KC = 30$ and different values of m

depth is quite close to the pure-wave case; as m is increased beyond $m = 0.4$–0.5, the scour depth increases, and for $m \geq 0.5$, the scour depths are effectively very similar to those in pure-current flows. These findings are again consistent with the experimental results of Sumer and Fredsøe (1996). There is, however, a tendency for the modeled equilibrium scour depths to be slightly larger than predicted by Eq. (13) (i.e., toward the upper limit of the standard deviation) in cases where m is high. This is as expected because $\theta_{cw} > 0.15$ in such cases, hence these results are consistent with the steady-current results shown in Fig. 4, where the equilibrium scour depth lies in the range of $0.8 < S_e/D < 0.9$ when $\theta > 0.15$. The same argument explains why the cases with $KC = 35$ also lie close to the upper limit of the standard deviation, because these cases, likewise, all result in high far-field Shields parameters.

Scour Profiles

The present section details the various types of equilibrium scour profiles that develop within the combined wave-plus-current scour simulations, as well as describes the range of flow conditions under which each type emerges. The results of the present numerical study have shown that combined current and wave climates can yield a variety of equilibrium profile shapes, depending on the combination of KC and m. In what follows, three different profile classes are identified, which can be characterized as follows: (1) those resembling profiles seen in steady currents, (2) those resembling profiles seen in pure waves, and (3) those markedly different from that observed in either pure-current or pure-wave climates, to be described in more detail.

Profiles resembling those from steady-current scour emerge in cases where the parameter m is large, typically $m \geq 0.6$, as should be intuitively expected. Perhaps more surprisingly, such profiles have also been identified in simulations with somewhat lower $m \geq 0.4$, provided that $KC \geq 35$. The development in the latter cases (i.e., with moderate m combined with sufficiently large KC) can be attributed to the large stroke of the wave, which induces pronounced erosion beneath the pipeline when the oscillatory flow follows, rather than opposes, the current. Examples of the scour profile developed under both scenarios are depicted in Fig. 9. Although KC and m are rather different, the resulting bed profiles for these two cases in the vicinity of the pipeline are both quite similar to those seen previously in pure-current flows (Fig. 3). Some differences emerge further away from the pipeline, especially downstream of the pipeline. Here, the shoulder in the current-dominated case [Fig. 9(a)] is almost completely eroded, whereas the shoulder is more pronounced in the case with an intermediate value of m [Fig. 9(b)].

In Fig. 10, equilibrium profiles from three different cases with low $m = 0.2$ are shown. For such low values of m, the resulting equilibrium scour profiles closely resemble those for pure waves, as expected. These are characterized by general profile symmetry in the vicinity of the pipeline, although some asymmetry develops further away, primarily in the form of one shoulder being larger than the other. In the pure-wave cases, as well as those with $m = 0.1$, this study's results suggest that the larger shoulder can emerge on either side of the pipeline. Alternatively, cases with $0.2 \leq m \leq 0.3$ primarily have a larger upstream shoulder, because emerging downstream shoulders tend to migrate downstream before slowly eroding as they become more exposed. This process can occur repeatedly as part of the dynamic equilibrium alluded to previously. A snapshot of this process can be seen in Fig. 10(a), where a new shoulder has just emerged (marked A), while the remnant of the previously developed shoulder (marked B) can still be seen migrating further downstream. In Fig. 10(b), the downstream shoulder has been completely washed away and a new one is about to form, whereas in Fig. 10(c), the downstream shoulder is close to maximum size and is just beginning to migrate downstream.

For intermediate values of m and $KC \leq 30$, the present model results suggest that the scour profile can differ markedly from those

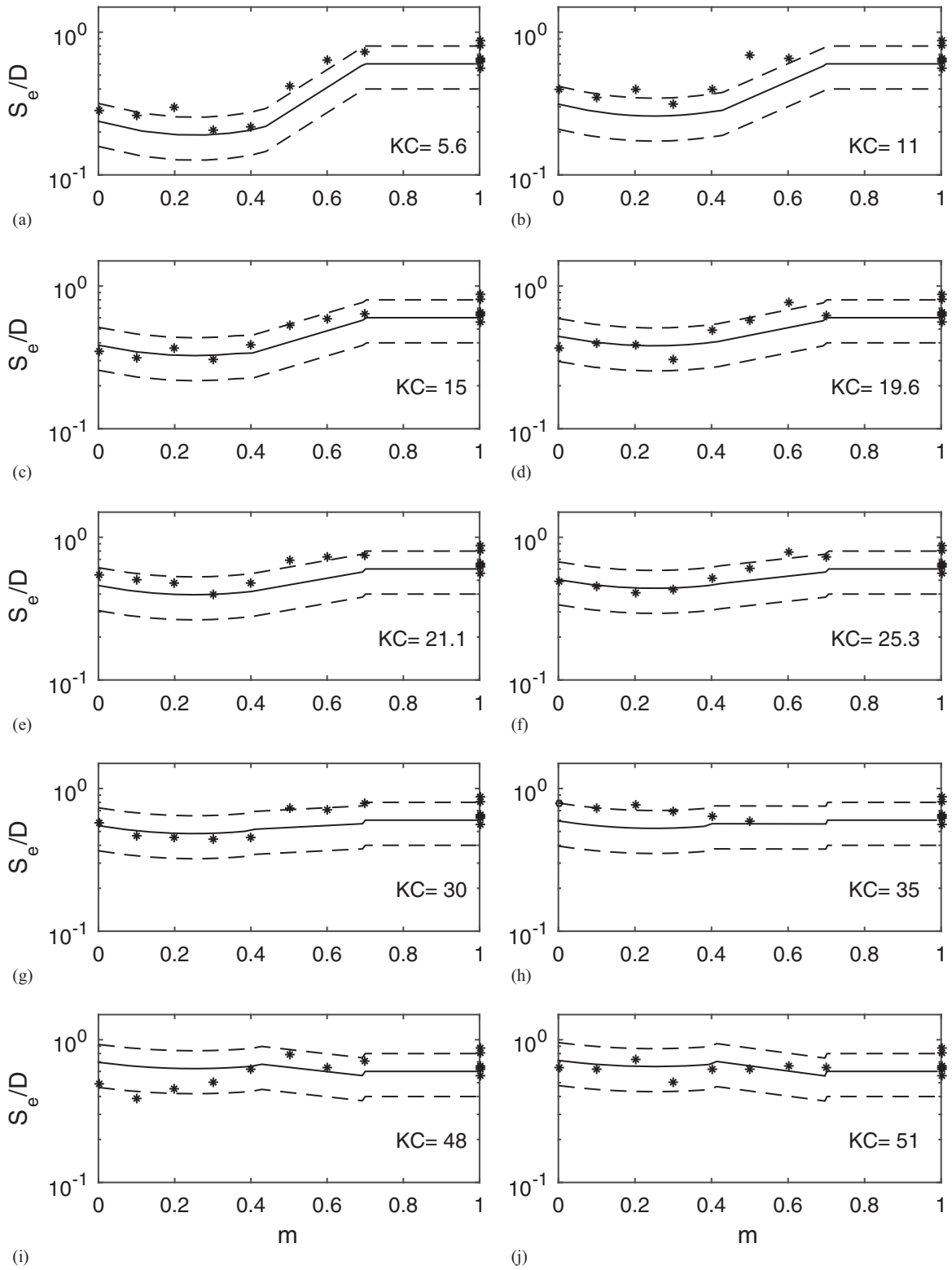

Fig. 8. Equilibrium scour depths: solid lines = empirical expression [Eq. (13)] from Sumer and Fredsøe (1996); asterisks = results from the present numerical simulations; dashed lines = standard deviation implied by incorporation of Eq. (4) in Eq. (13)

typical of either pure-wave or pure-current conditions. Such profiles are characterized by a downstream shoulder much closer to the pipeline than the upstream shoulder. Typical examples are illustrated in Fig. 11, where profiles for three different values of *KC* with intermediate values of *m* are shown. Given the relative strength of the current in these cases, these profiles can be considered as somewhat counterintuitive, as the mean flow might have been expected to drive the downstream shoulder away from the pipeline. The sequence leading to the emergence of such profiles can be described as follows. During early stages of the scour process, a small shoulder develops downstream of the pipeline. With time this shoulder continues to grow, eventually causing flow separation on the lee side.

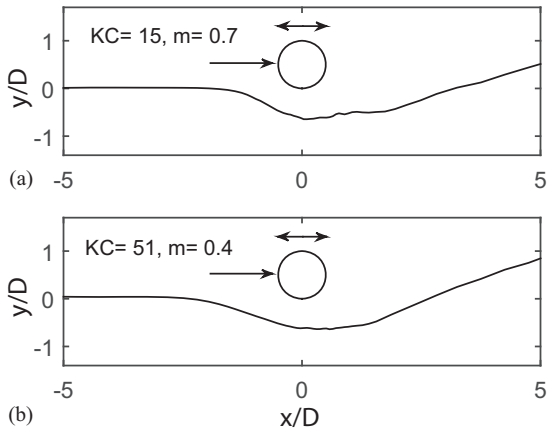

Fig. 9. Equilibrium scour profile of (a) $KC = 15$, $m = 0.7$ and (b) $KC = 51$, $m = 0.4$

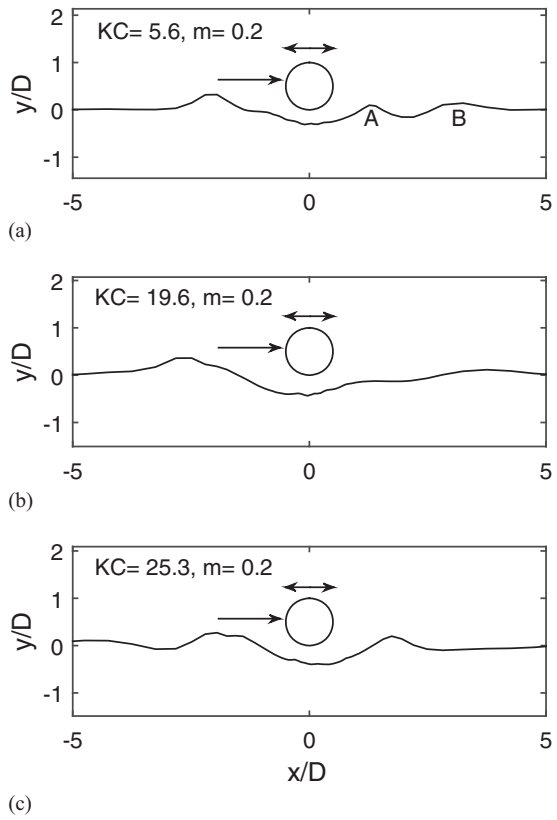

Fig. 10. Equilibrium scour profile of (a) $KC = 5.6$, $m = 0.2$; (b) $KC = 19.6$, $m = 0.2$; and (c) $KC = 25.3$, $m = 0.2$

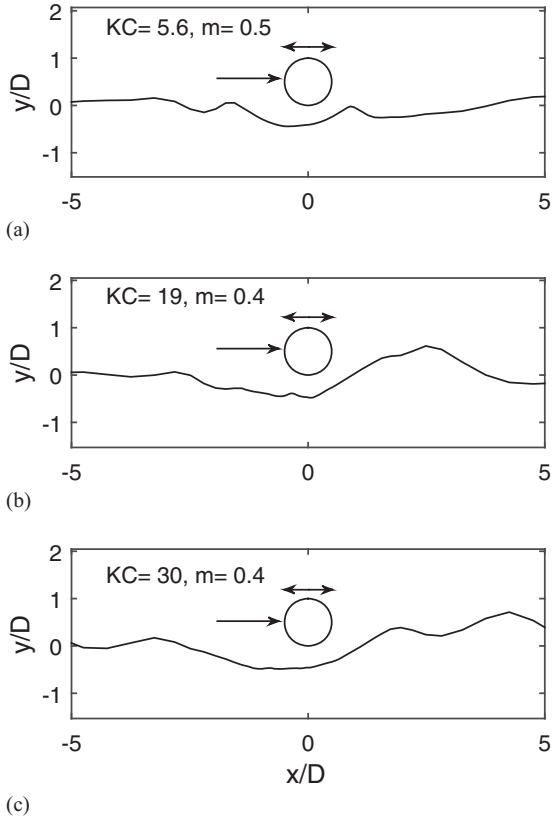

Fig. 11. Equilibrium scour profile of (a) $KC = 5.6$, $m = 0.5$; (b) $KC = 19.6$, $m = 0.4$; and (c) $KC = 30$, $m = 0.4$

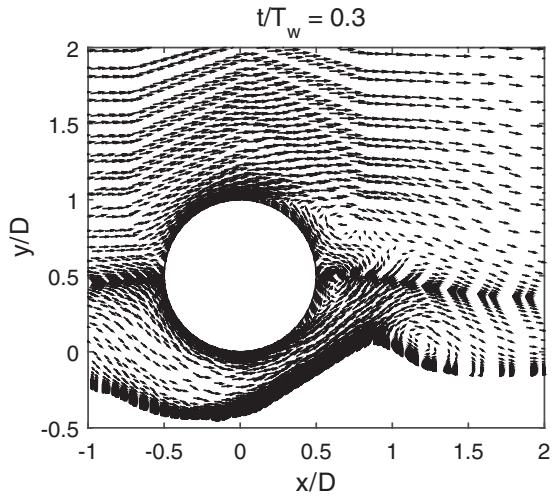

Fig. 12. Instantaneous velocity fields in the case of $KC = 5.6$, $m = 0.5$

This creates a lee-side vortex, which in turn causes additional growth, and eventual stability, of the shoulder. The flow patterns just described are illustrated in Fig. 12, where the instantaneous velocity field is plotted for the case with $KC = 5.6$ and $m = 0.5$ at $t/T_w = 0.3$. In these cases, the vortices shed from the bottom of the pipeline are relatively weak, hence limiting the lee-wake erosion. As experimental confirmation for this type of profile, one observed by Sumer and Fredsøe (1996) with $KC = 10$ and $m = 0.48$ is shown in Fig. 13. Here, it can be seen that the observed experimental profile shape is indeed very similar to that from the model with similar parameters (i.e., $KC = 5.6$, $m = 0.5$), depicted in Fig. 11(a) for example.

Timescale

The timescale of scour qualitatively represents the time required for significant scour to develop. Being a fundamental quantity necessary for predicting the time sequence of scour beneath pipelines, this quantity is of significant engineering importance (e.g., in the

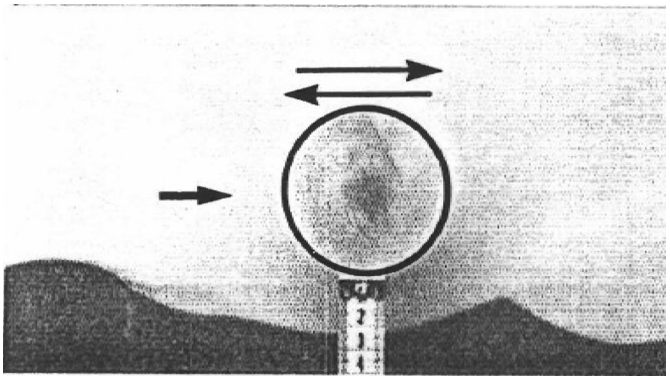

Fig. 13. Equilibrium scour profile of $KC = 10$, $m = 0.48$ (reprinted with permission from Sumer and Fredsøe 1996)

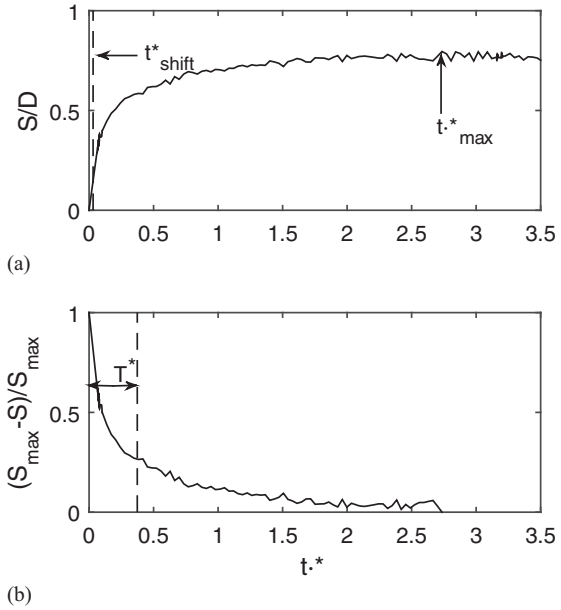

Fig. 14. Example of the calculation of the scour timescale T^* for $KC = 19.6$ with $m = 0.6$

fatigue life assessment of submarine pipelines). Although practical methods exist (see Fredsøe and Deigaard 1992; Sumer and Fredsøe 2002, p. 72) for predicting the scour time scale in both pure-current as well as pure-wave conditions, this quantity has not previously been investigated and properly parameterized for generalized wave-plus-current flow environments, to the authors' knowledge. This knowledge gap will be filled by analyzing the full matrix of numerical results in the present section.

In what follows, the scour timescales for all simulated cases have been determined by integration of the scour curves. Because an initial scour hole was prescribed, the time used for the integration then corresponds to the shifted time ($t'^* = t^* + t^*_{\text{shift}}$), with the dimensionless timescale then calculated according to

$$T^* = \frac{\sqrt{g(s-1)d^3}}{D^2} T = \int_0^{t'^*_{\max}} \frac{S_{\max} - S}{S_{\max}} dt'^*, \tag{17}$$

as suggested by Fuhrman et al. (2014), where T = dimensional timescale. An example for both the backward extrapolation of the scour

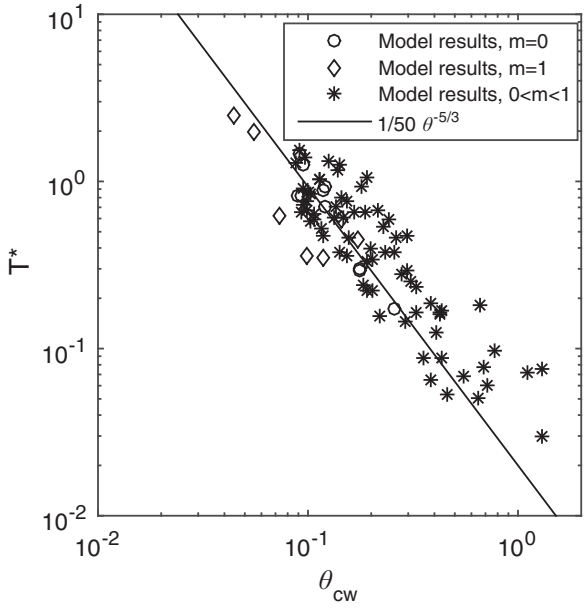

Fig. 15. Timescale of the scour development in the combined waves and current case

curve as well as the integrated quantity with respect to time is shown in Figs. 14(a and b). As seen there, the time shift necessary due to the initial scour profile used in the simulations does not typically make a major contribution to the timescale.

As a first attempt at parameterization of the wave-plus-current scour timescale, Fig. 15 shows the computed nondimensional timescales as a function of θ_{cw} for all cases considered in the present work. As a reference, the experimentally based relation for the timescale of Fredsøe and Deigaard (1992)

$$T^* = \frac{1}{50} \theta^{-\frac{5}{3}} \tag{18}$$

is also shown as the full line, which was demonstrated to be valid for both pure-current as well as pure-wave scour conditions. Fig. 15 shows that both the pure-current (diamonds, $m = 1$) and especially the pure-wave (circles, $m = 0$) results match the reference line [Eq. (18)] reasonably, which is generally consistent with the experimental findings of Fredsøe and Deigaard (1992). Alternatively, the combined wave-plus-current results (asterisks, $0 < m < 1$) consistently lie either very close to or above the full line [Eq. (18)], implying a generally increased timescale for a given maximum Shields parameter, relative to either the pure-current or pure-wave limit.

Such an increase in the timescale (i.e., reduced scour rates) under combined wave-plus-current conditions should in fact be expected on physical grounds. A simple explanation is as follows: when m is higher than approximately 0.5, the free stream flow becomes unidirectional, oscillating between a strong and a weak current. In this way, it is effectively working like a strong current that is being periodically increased and decreased. This results in significant sediment transport, and hence scour, during the first half-period and much less during the second half-period. This behavior is quantitatively illustrated in Fig. 16, where the free-stream velocity and scour time series over the first two periods for the case with $KC = 15$ and $m = 0.6$ are shown. The resulting *pump effect* can clearly be seen directly in the velocity time series, as well as indirectly via the stepwise increase in the scour depth Fig. 16 (i.e., increasing scour when the flow is near maximum, followed by virtually no scour when the

flow is near minimum). From the aforementioned description, it must be expected that the scour in a pure-current case with the same maximum Shields parameter will develop faster than in a combined wave-plus-current case, where the flow is near maximum for only a fraction of the overall time. Note that similar arguments might also be made for the pure-wave scour situations. However, in such cases, significant sediment is being transported in both directions (i.e., twice per wave period). Moreover, the largely symmetric profile shape in wave-dominated flows is also quite different than for cases involving current-dominated flows (i.e., those involving high values of m), as established previously. From the previous findings, it is clear that the timescale T^* must depend not only on the Shields parameter (θ_{cw}) but also on m for generalized wave-plus-current situations. The Shields parameter (θ_{cw}) is obviously important, as it governs the maximum sediment transport, and hence scour, rates. Given that the nondimensional timescale at both pure-wave and pure-current limits scales as $\theta^{-5/3}$ [see again Eq. (18)], similar scaling should be expected in combined wave–current cases, as will be confirmed. Additionally, m dependence must also be included to account for the flow and scour rates being near maximum for only a limited fraction of the time. It can likewise be surmised that the timescale should not depend on KC, given that it depends only on θ even in the pure-wave cases [see again Eq. (18)]. Following those arguments, the timescale of the combined wave-plus-current cases will now be generalized to

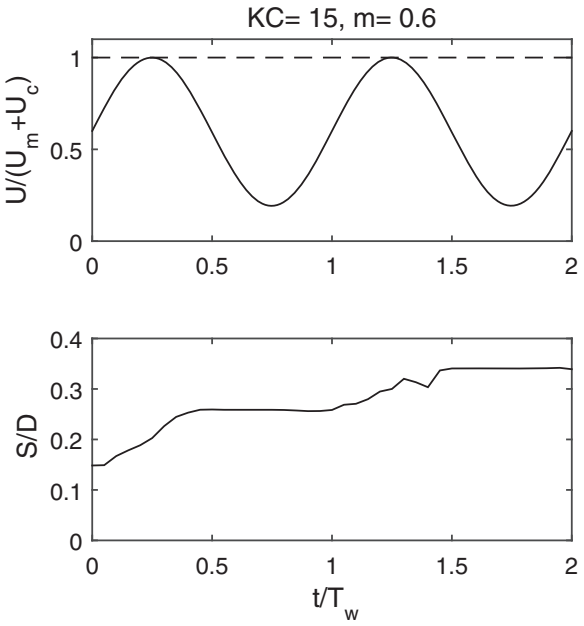

Fig. 16. Scour time and free-stream velocity time series of $KC = 15$ with $m = 0.6$; dashed line indicates the steady-current situation having the same maximum velocity as the combined case

$$T^* = \Gamma(m)\theta_{cw}^{-\frac{5}{3}}, \tag{19}$$

for predicting the scour timescale in combined wave-plus-current flows, where $\Gamma(m)$ = (as yet undetermined) function of m.

To begin determining $\Gamma(m)$, the computed dimensionless timescales (T^*) from Fig. 15 are plotted against θ_{cw} in Fig. 17, with results for various KC now grouped separately according to each of the discrete m considered. On each subfigure, the target [Eq. (19)] is also plotted (full lines), utilizing a constant value for $\Gamma(m)$ selected to best fit the individual data sets for each m. The only exceptions are those with $m = 0$ and $m = 1$, corresponding to pure-wave and

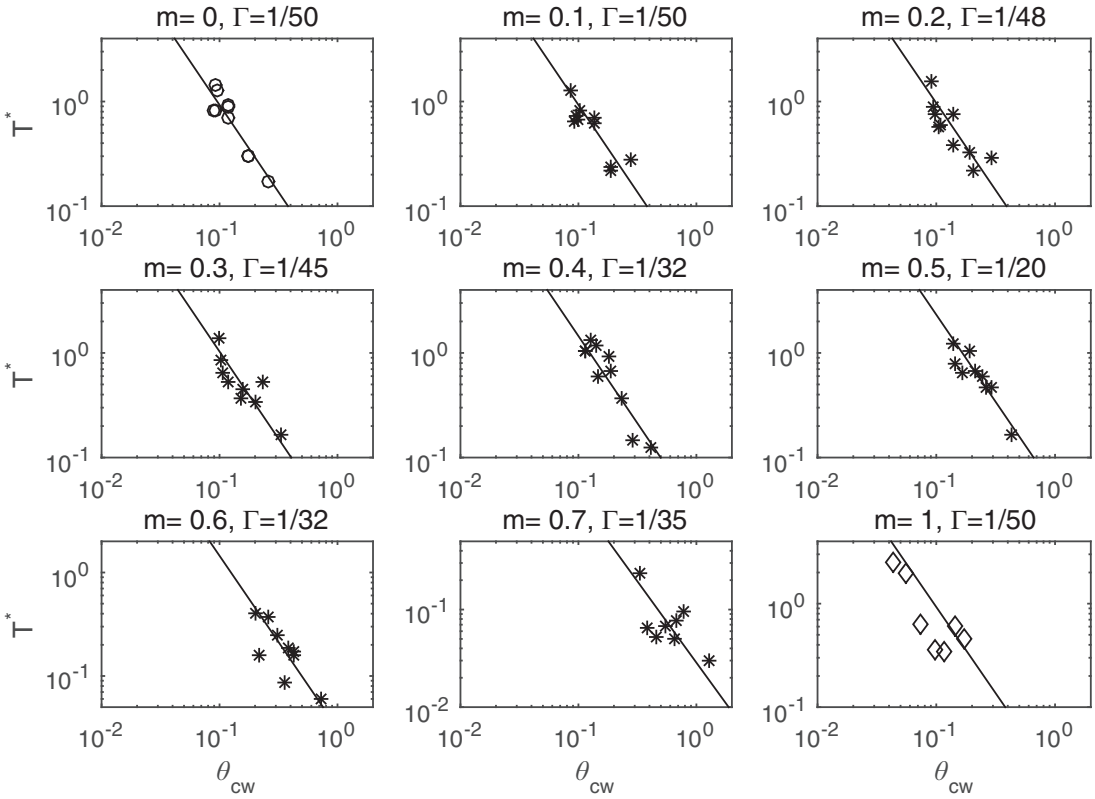

Fig. 17. Fit of the modeled timescales and Eq. (19)

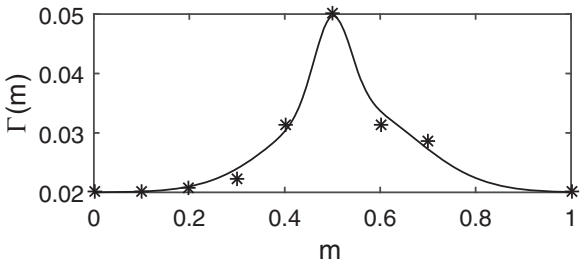

Fig. 18. Fit between (line) the suggested function for $\Gamma(m)$ [Eq. (20)] and (asterisk) the estimated values for $\Gamma(m)$

pure-current cases, respectively, where $\Gamma(m) = 1/50$ is utilized for consistency with Eq. (18). This also yields reasonable fits, as shown here and previously. It can be seen that Eq. (19), with properly selected $\Gamma(m)$ values, gives a quite good approximation for all cases (i.e., spanning the full range of m). Although there is inevitably some scatter in the results, this appears to be of the same order of magnitude as typically seen in experiments (see Fredsøe and Deigaard 1992).

Inspired by the previous findings, the authors sought a closed-form expression for the function $\Gamma(m)$. The best-fit values for $\Gamma(m)$ for each discrete m from Fig. 17 are plotted as asterisks in Fig. 18. Also shown as the full line is the function

$$\Gamma(m) = \frac{1}{50} + 0.015\left(e^{-350(m-0.5)^2} + e^{-25(m-0.53)^2}\right) \tag{20}$$

which matches the discrete values very well while also tending naturally to the experimentally based $\Gamma(m) = 1/50 = 0.02$ at both the $m = 0$ and $m = 1$ limits, again consistent with Eq. (18). Fig. 18 shows that $\Gamma(m)$ increases with m over the range $0 \le m \le 0.5$, meaning that the scour timescale is larger than in pure-wave or pure-current cases. The function $\Gamma(m)$ then peaks at $m = 0.5$, before decreasing back to the steady-current value at $m = 1$. All of these results are generally consistent with the physical considerations discussed previously.

As a final check of the results, the computed timescale results from Fig. 15 are recast in Fig. 19, now in a form consistent with Eq. (19), i.e., as $T^*/\Gamma(m)$ versus θ_{cw}, while invoking Eq. (20). It is now seen that the considerable scatter previously evident in Fig. 15 for the combined wave-plus-current results is now significantly reduced. The tight clustering around the full line in Fig. 19 hence confirms that the generalized expression in Eq. (19) combined with Eq. (20) effectively unites the simulated timescales for pure-current, pure-wave, as well as the combined wave-plus-current flows.

Based on the full consistency with the existing experimentally based expression [Eq. (18)], the large matrix of physical conditions considered, as well as the good agreement between model and measured scour processes presented here [Eq. (19)], is believed to be appropriate for the engineering prediction of the scour timescale beneath pipelines for general wave-plus-current flows.

Example Calculations

An example of how to calculate both the timescale of the scour development and the equilibrium scour depth in combined wave and current climates is given. Consider a situation with a $D = 30$ cm pipeline laid on the seabed exposed to waves with a period of $T_w = 10$ s, a wave height of $H = 2$ m, a water depth of $h = 10$ m, and a

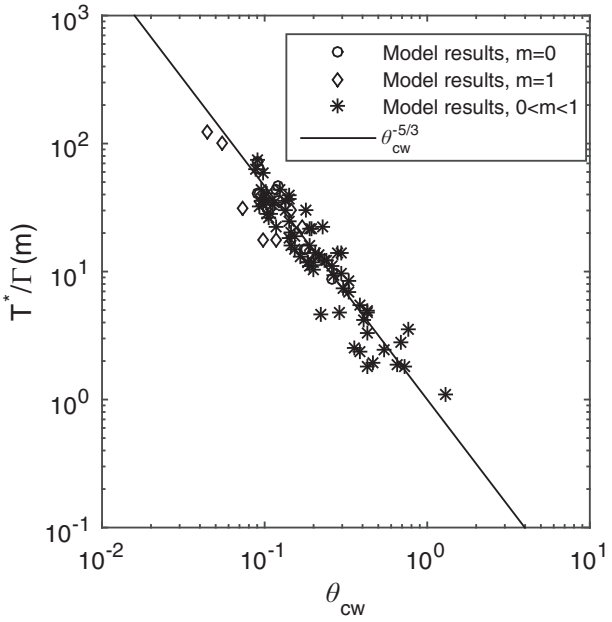

Fig. 19. Timescale in the combined wave-current flow as a function of the Shields parameter

mean current of $V = 0.6$ m/s. The grain size is $d = 0.5$ mm with a relative density of $s = 2.65$. Note that these combine the conditions of the pure-wave and pure-current examples in Sumer and Fredsøe (2002, pp. 46–48, 72–75).

Timescale

1. Calculate U_m utilizing linear wave theory by first calculating the wave number (k) by solving the linear dispersion relation

$$\left(\frac{2\pi}{T_w}\right)^2 = gk\tanh(kh) \Rightarrow k = 0.068\ \mathrm{m}^{-1}$$

and then inserting into

$$U_m = \frac{\pi H}{T_w}\frac{\cosh(kz)}{\sinh(kh)} = 0.86\ \mathrm{m/s}$$

where $z = 0$ is the distance from the bottom.

2. Estimate the maximum friction velocity of the wave (U_{fw}) by inserting into Eq. (9) by first finding the friction factor (f_w) according to $f_w = \max[f_w^{\mathrm{lam}}, f_w^{\mathrm{smooth}}, f_w^{\mathrm{rough}}]$, where $f_w^{\mathrm{lam}} = 0.0019$ is found from Eq. (10), $f_w^{\mathrm{smooth}} = 0.0037$ is calculated from Eq. (11), and $f_w^{\mathrm{rough}} = 0.0074$ is calculated from Eq. (12). Taking $f_w = f_w^{\mathrm{rough}}$ yields $U_{fw} = 0.052$ m/s.
3. Calculate the friction velocity from the current alone by the flow resistance formula

$$U_{fc} = \frac{V\kappa}{\left(\ln\left(\frac{30h}{k_s}\right) - 1\right)} = 0.021\ \mathrm{m/s}$$

where $\kappa = 0.4$ is the von Karman constant.
4. Estimate the velocity at the pipeline center (U_c) by assuming a rough logarithmic velocity profile

$$U_c = \frac{U_{fc}}{\kappa}\left(\ln\left(\frac{30\frac{D}{2}}{k_s}\right)\right) = 0.43\,\mathrm{m/s}$$

Inserting this into Eq. (6) then yields the nondimensional parameter $m = 0.34$.

5. Calculate the Shields parameter of the wave $\theta_w = 0.34$ and the current $\theta_{cur} = 0.055$ by inserting U_{fw} and U_{fc} in Eq. (2). Insert these into Eq. (8) to calculate $\theta_m = 0.095$.
6. Calculate the characteristic undisturbed Shields parameter (θ_{cw}) from Eq. (7). This gives $\theta_{cw} = 0.43$.
7. Insert m into Eq. (20) to get $\Gamma = 0.026$ and insert this as well as θ_{cw} into Eq. (19) to get $T^* = 0.10$.
8. Finally, calculate the actual timescale from Eq. (17), giving $T = 210\ \mathrm{s} \approx 3.5$ min.

For comparison, repeating the calculations with the naive approach [i.e., inserting θ_{cw} into Eq. (18)] yields $T = 162\ \mathrm{s} \approx 2.7$ min, which is somewhat faster.

Scour Depth

1. From Eq. (5), calculate $KC = 28.5$.
2. Calculate $a_m = 0.55$ from Eq. (15) and $b_m = -1.12$ from Eq. (16). From Eq. (14), one finds $F = 0.80$.
3. Insert F as well as Eq. (4) into Eq. (13) to get $S_e/D = 0.48 \pm 0.16$ or $S_e = 0.14 \pm 0.05$ m.

Conclusions

In this work, results from a fully coupled hydrodynamic and morphodynamic CFD model for simulating wave-plus-current–induced scour beneath submarine pipelines have been presented. The hydrodynamic model solves the incompressible RANS equations, coupled with k-ω turbulence closure. The model includes both bed and suspended load sediment transport descriptions, which drive seabed morphology based on the sediment continuity equation. A sand-slide model is likewise incorporated, thus ensuring that the angle of repose is not exceeded on the seabed.

The model has been validated through comparison against the experimental results of Mao (1986), who investigated scour beneath pipelines in steady-current flows. The model has demonstrated the ability to accurately reproduce the profile shape evolution during the scour process in both clear-water and live-bed scour regimes. The model has likewise demonstrated the ability to yield equilibrium scour depths in good agreement with those observed by Mao (1986) over a wide range of Shields parameters. The present validation results for the scour induced by steady-current–induced flows are complemented by those recently presented by Fuhrman et al. (2014) involving wave-induced scour processes.

The validated model has been subsequently utilized for the simulation of wave-plus-current–induced scour involving 10 wave environments (characterized by KC numbers ranging from 5.6 to 51) in combination with up to eight current environments (characterized by a current-strength parameter m ranging from 0 to 0.7, where $m = 0$ and $m = 1$, respectively, correspond to the pure-wave and pure-current limits). The model successfully predicts equilibrium scour depths and trends in general accordance with the experimentally based empirical expressions for combined wave-current flows developed by Sumer and Fredsøe (1996) over the full range considered, serving as further validation.

The model results suggest that, in wave-dominated flows (low m), the emerging scour profiles expectedly resemble those induced by pure-wave environments, whereas those emerging in current-dominated flows (medium to large m, depending somewhat on KC) closely resemble those induced by pure-current environments. Additionally, the model results suggest that situations having intermediate m (i.e., situations that are neither wave- nor current-dominated) can result in equilibrium profiles characterized by a downstream shoulder closer to the pipeline than the upstream shoulder. This profile type has been reconciled directly with experimental observations of Sumer and Fredsøe (1996).

The matrix of simulated scour cases has been utilized to systematically investigate the scour timescale within combined wave-current flows. For a given maximum Shields parameter, it is found that the dimensionless scour timescale for wave-plus-current environments is larger than for pure-current situations. This has been simply explained as due to the Shields parameter being near maximum for only a small fraction of the total time during combined wave-current flows. Systematic assessment of the scour time series, grouped by discrete values of m, has resulted in a new and generalized analytical expression for the combined wave-plus-current dimensionless timescale. This is of the form $T^* = \Gamma(m)\theta_{cw}^{-\frac{3}{2}}$, where the function $\Gamma(m)$ is given in closed form within the paper. Importantly, this function tends to $\Gamma(m) = 1/50$ for both pure-wave and pure-current flows, hence unifying existing experimentally based expressions for the timescale at these limits (Fredsøe and Deigaard 1992). The resulting expression has been shown to match well the full range of simulated timescales considered. Given the demonstrated collective accuracy of the model in simulating scour processes as a result of currents, waves (Fuhrman et al. 2014), as well as their combination, it is believed that the proposed expression for the generalized wave-plus-current scour timescale is appropriate for engineering use.

Acknowledgments

The authors acknowledge support from the European Union Project ASTARTE [Assessment, Strategy and Risk Reduction for Tsunamis in Europe; Grant No. 603839 (FP7-ENV-2013.6.4-3)]. The third author additionally acknowledges Innovative Multipurpose Offshore Platforms: Planning, Design and Operation (MERMAID), 20122016, Grant Agreement No. 288710 of European Commission, 7th Framework Programme for Research.

References

Baykal, C., Sumer, B. M., Fuhrman, D. R., Jacobsen, N. G., and Fredsøe, J. (2015). "Numerical investigation of flow and scour around a vertical circular cylinder." *Philos. Trans. A Math. Phys. Eng. Sci.*, 373(2033), 1–21.

Bernetti, R., Bruschi, R., Valentini, V., and Ventur, M. (1990). "Pipelines placed on erodible seabeds." *Proc., 9th Int. Conf. on Offshore Mechanics and Arctic Engineering*, Vol. 5, ASME, Houston, 155–164.

Brørs, B. (1999). "Numerical modeling of flow and scour at pipelines." *J. Hydraul. Eng.*, 10.1061/(ASCE)0733-9429(1999)125:5(511), 511–523.

Cebeci, T., and Chang, K. C. (1978). "Calculation of incompressible rough-wall boundary-layer flows." *AIAA J.*, 16(7), 730–735.

Cheng, L., Yeow, K., Zang, Z., and Li, F. (2014). "3D scour below pipelines under waves and combined waves and currents." *Coastal Eng.*, 83, 137–149.

Engelund, F., and Fredsøe, J. (1976). "A sediment transport model for straight alluvial channels." *Nordic Hydrol.*, 7(5), 293–306.

Fredsøe, J., Andersen, K. H., and Sumer, B. M. (1999). "Wave plus current over a ripple-covered bed." *Coastal Eng.*, 38(4), 177–221.

Fredsøe, J., and Deigaard, R. (1992). *Mechanics of coastal sediment transport*, World Scientific, Singapore.

Fredsøe, J., Sumer, B. M., and Arnskov, M. M. (1992). "Time scale for wave/current scour below pipelines." *Int. J. Offshore Polar Eng.*, 2(1), 13–17.

Fuhrman, D. R., Baykal, C., Sumer, B. M., Jacobsen, N. G., and Fredsøe, J. (2014). "Numerical simulation of wave-induced scour and backfilling processes beneath submarine pipelines." *Coastal Eng.*, 94, 10–22.

Fuhrman, D. R., Schløer, S., and Sterner, J. (2013). "RANS-based simulation of turbulent wave boundary layer and sheet-flow sediment transport processes." *Coastal Eng.*, 73, 151–166.

Hansen, E. A. (1992). "Scour below pipelines and cables: A simple model." *Proc., 11th Offsjore Mechanics and Arctic Engineering Conf.*, Vol. V, ASME, New York, 133–138.

Hoffmans, G. J. C. M., and Verheij, H. J. (1997). *Scour manual.* A.A. Balkema, Rotterdam, The Netherlands.

Jacobsen, N. G., Fredsoe, J., and Jensen, J. H. (2014). "Formation and development of a breaker bar under regular waves. Part 1: Model description and hydrodynamics." *Coastal Eng.*, 88, 182–193.

Jacobsen, N. G., Fuhrman, D. R., and Fredsøe, J. (2012). "A wave generation toolbox for the open-source CFD library: OpenFoam (R)." *Int. J. Numer. Methods Fluids*, 70(9), 1073–1088.

Kazeminezhad, M. H., Yeganeh-Bakhtiary, A., Etemad-Shahidi, A., and Baas, J. H. (2012). "Two-phase simulation of wave-induced tunnel scour beneath marine pipelines." *J. Hydraul. Eng.*, 10.1061/(ASCE)HY.1943-7900.0000540, 517–529.

Liang, D., and Cheng, L. (2005a). "Numerical model for wave-induced scour below a submarine pipeline." *J. Waterway Port, Coastal, Ocean Eng.*, 10.1061/(ASCE)0733-950X(2005)131:5(193), 193–202.

Liang, D., and Cheng, L. (2005b). "Numerical modeling of flow and scour below a pipeline in currents Part I. Flow simulation." *Coastal Eng.*, 52(1), 25–42.

Liang, D., Cheng, L., and Li, F. (2005). "Numerical modeling of flow and scour below a pipeline in currents: Part II. Scour simulation." *Coastal Eng.*, 52(1), 43–62.

Lucassen, R. J. (1984). "Scour underneath submarine pipelines." *Rep. No. PL-4 2A*, Netherlands Marine Technical Research, Netherlands Industrial Council for Oceanology, Delft Univ. of Technology, Delft, The Netherlands.

Mao, Y. (1986). *The interaction between a pipeline and an erodible bed.* Series Paper No. 39, Institute of Hydrodynamic and Hydraulic Engineering, Technical Univ. of Denmark, Copenhagen, Denmark.

Myrhaug, D., Ong, M. C., Føien, H., Gjengedal, C., and Leira, B. J. (2009). "Scour below pipelines and around vertical piles due to second-order random waves plus current." *Ocean Eng.*, 36(8), 605–616.

OpenFOAM [Computer software]. The OpenFOAM Foundation, London.

Roulund, A., Sumer, B. M., Fredsøe, J., and Michelsen, J. (2005). "Numerical and experimental investigation of flow and scour around a circular pile." *J. Fluid Mech.*, 534, 351–401.

Soulsby, R. L. (1995). "Bed shear-stresses due to combined waves and currents." *Advances in coastal morphodynamics*, M. J. F. Stive, H. D. Vriend, J. Fredsøe, L. Hamm, R. L. Soulsby, C. Teisson, and J. C. Winterwerp, eds., Delft Hydraulics, Delft, The Netherlands, 4–20 to 4–23.

Sumer, B. M., and Fredsøe, J. (1990). "Scour below pipelines in waves." *J. Waterway, Port, Coastal, Ocean Eng.*, 10.1061/(ASCE)0733-950X(1990)116:3(307) 307–323.

Sumer, B. M., and Fredsøe, J. (1996). "Scour around pipelines in combined waves and current." *Proc., Int. Conf. on Offshore Mechanics and Arctic Engineering - OMAE*, G. Rosa, ed., Vol. 5, ASME, New York, 595–602.

Sumer, B. M., and Fredsøe, J. (2002). *The mechanics of scour in the marine environment*, World Scientific, Singapore.

Whitehouse, R. (1998). *Scour at marine structures: A manual for practical applications*, Thomas Telford Ltd., London.

Wilcox, D. C. (2006). *Turbulence modeling for CFD*, 3rd Ed., DCW Industries, Inc., La Canada, CA.

Wilcox, D. C. (2008). "Formulation of the k-ω turbulence model revisited." *AIAA J.*, 46(11), 2823–2838.

Zanganeh, M., Yeganeh-Bakhtiary, A., and Wahab, A. K. A. (2012). "Lagrangian coupling two-phase flow model to simulate current-induced scour beneath marine pipelines." *Appl. Ocean Res.*, 38, 64–73.

Zhao, Z., and Fernando, H. J. S. (2007). "Numerical simulation of scour around pipelines using an euler-euler coupled two-phase model." *Environ. Fluid Mech.*, 7(2), 121–142.